Mon. Not. R. Astron. Soc. **000**, 1–15 (2010) Printed 16 April 2015 (MN LATEX style file v2.2)

# Expanded haloes, abundance matching and too-big-to-fail in the Local Group

Chris B. Brook[1⋆] & Arianna Di Cintio[1,2]†
[1]*Departamento de Física Teórica, Módulo C-15, Facultad de Ciencias, Universidad Autónoma de Madrid, 28049 Cantoblanco, Madrid, Spain*
[2]*Dark Cosmology Centre, Niels Bohr Institute, University of Copenhagen, Juliane Maries Vej 30, DK-2100 Copenhagen, Denmark*

arXiv:1410.3825v2 [astro-ph.GA] 15 Apr 2015

Accepted XXXX . Received XXXX; in original form XXXX

**ABSTRACT**

Observed kinematical data of 40 Local Group (LG) members are used to derive the dark matter halo mass of such galaxies. Haloes are selected from the theoretically expected LG mass function and two different density profiles are assumed, a standard universal cuspy model and a mass dependent profile which accounts for the effects of baryons in modifying the dark matter distribution within galaxies. The resulting relations between stellar and halo mass are compared with expectations from abundance matching.

Using a universal cuspy profile, the ensemble of LG galaxies is fit in relatively low mass haloes, leaving "dark" many massive haloes of $\mathrm{M_{halo}}\gtrsim10^{10}\mathrm{M_\odot}$: this reflects the "too big to fail" problem and results in a $\mathrm{M_{star}}$-$\mathrm{M_{halo}}$ relation that differs from abundance matching predictions. Moreover, the star formation efficiency of isolated LG galaxies increases with decreasing halo mass when adopting a cuspy model. By contrast, using the mass dependent density profile, dwarf galaxies with $\mathrm{M_{star}}\gtrsim10^{6}\mathrm{M_\odot}$are assigned to more massive haloes, which have a central cored distribution of dark matter: the "too big to fail" problem is alleviated, the resultant $\mathrm{M_{star}}$-$\mathrm{M_{halo}}$ relation follows abundance matching predictions down to the completeness limit of current surveys, and the star formation efficiency of isolated members decreases with decreasing halo mass, in agreement with theoretical expectations.

Finally, the cusp/core space of LG galaxies is presented, providing a framework to understand the non-universality of their density profiles.

**Key words:** galaxies: formation - haloes - Local Group - dwarf

## 1 INTRODUCTION

The $\Lambda$ Cold Dark Matter ($\Lambda$CDM) model has been successful in explaining a multitude of observations at cosmological scales, such as anisotropies of Cosmic Microwave Background radiation (CMB) (e.g. Jarosik & et al. 2011) and galaxy clustering on large scales (e.g. Cole & et al. 2005). However, the $\Lambda$CDM model has problems on galactic scales, such as the "missing satellite problem", the "too big to fail" problem and the "cusp-core" discrepancy. At these small scales, tests of the $\Lambda$CDM model are complicated by astrophysical processes involved in galaxy formation.

The "missing satellite problem", which is the discrepancy between the number of observed satellites and the number of predicted dark matter sub-haloes (Klypin et al. 1999; Moore et al. 1999), can be resolved if the lowest mass dark matter haloes are inefficient at forming stars due to the early reionization of the intergalactic medium (Bullock et al. 2000; Somerville 2002; Benson et al. 2002).

Yet there remains a mismatch between the predicted and observed kinematics of galaxies in the mass range where haloes are too massive to have star formation suppressed by reionization processes, i.e. they are "too big to fail" (Boylan-Kolchin et al. 2011). A lack of observed galaxies with the kinematics expected for such haloes has been reported in satellites of the Milky Way (MW) and Andromeda (M31) (Boylan-Kolchin et al. 2012; Collins et al. 2014; Tollerud et al. 2014), in the Local Group (Ferrero et al. 2012; Garrison-Kimmel et al. 2014a; Kirby et al. 2014) and in the velocity function within the local volume, as measured by HI line widths (Klypin et al. 2014; Papastergis et al. 2015). High resolution rotation curves of dwarf galaxies from the THINGS survey (Oh et al. 2011a) and a sample of low mass ($10^7 < \mathrm{M_{star}/M_\odot} < 10^9$) star-forming galaxies at intermediate redshift (Miller et al. 2014) show a similar disagreement with theoretical expectations, since their observed kinematics indicate that their haloes are less massive than abundance matching (Guo et al. 2010; Moster et al. 2013) would suggest.

⋆ E-mail: cbabrook@gmail.com
† E-mail: arianna.dicintio@uam.es

© 2010 RAS

These discrepancies between theory and observation arise under the assumption that galaxies reside in dark matter haloes whose properties are derived from collisionless N-body cosmological simulations, i.e. their density profiles are steep, or "cuspy", toward the centre (Navarro et al. 1997). Such NFW profile implies that rotation curves of galaxies should increase rapidly with radius. However, there is ample evidence that observed rotation curves rise slowly, and that dwarf galaxies have flat, or "cored", inner density profiles (e.g., Moore 1994; Salucci & Burkert 2000; de Blok et al. 2001; Simon et al. 2005; Kuzio de Naray et al. 2008; Oh et al. 2011b). This is the well known "cusp-core" discrepancy.

Within a ΛCDM scenario, the "too big to fail" problem is likely a re-casting of the "cusp-core" discrepancy, with the mismatch between observed and theoretical velocities of massive dwarfs and satellites reflecting the existence of cores in such galaxies. Therefore, a possible solution to both the "cusp-core" discrepancy *and* the "too big to fail" problem is the formation of cores through the effects of baryonic physics (Governato et al. 2012; Madau et al. 2014), such as the non-adiabatic impact of gas outflows on dark matter haloes (Navarro et al. 1996; Read & Gilmore 2005; Mashchenko et al. 2008; Pontzen & Governato 2012; Ogiya & Mori 2014)

There is significant observational evidence (Weiner et al. 2009; Martin et al. 2012) that energy feedback from star-formation activity drives gas out of galaxies. Processes such as radiation energy from massive stars, stellar winds and supernova explosions have been shown to play a central role in galaxy formation (Binney et al. 2001; Brook et al. 2011; Stinson et al. 2013; Hopkins et al. 2014).

Both simple analytic arguments (Brook & Di Cintio 2015 in prep) and detailed cosmological simulations (Di Cintio et al. 2014a) show that the degree of halo expansion due to outflows is dependent on the ratio of stellar to halo mass, $\mathrm{M_{star}/M_{halo}}$. Low mass galaxies are dark matter dominated: those with $\mathrm{M_{star}} \lesssim 3\text{-}5\times10^{6}\mathrm{M_{\odot}}$ do not produce enough energy to flatten the halo's inner density profile, which remains steep (Peñarrubia et al. 2012; Governato et al. 2012; Di Cintio et al. 2014a). As stellar mass increases relative to the dark matter mass, the inner density profile becomes increasingly flat (Governato et al. 2012; Di Cintio et al. 2014a). The flattening is greatest when $\mathrm{M_{star}} \sim 3\times10^{8}\mathrm{M_{\odot}}$, after which the deeper potential well is able to oppose the halo expansion (Di Cintio et al. 2014a,b), resulting in a profile which becomes steeper for more massive galaxies, and effectively returns to the NFW value at about the Milky Way mass.

While some scatter in the relation between inner slope and $\mathrm{M_{star}/M_{halo}}$ is certainly expected, due to the different evolution of galaxies, different star formation, merger histories and environments, at a first order the amount of stars per halo mass at redshift zero gives a good approximation of the energy from supernovae feedback, available to flatten the dark matter profiles, versus the total gravitational potential energy of the NFW halo.

Using the results from hydrodynamical galaxy formation simulations that match a wide range of galaxy scaling relations (Brook et al. 2012; Stinson et al. 2013) and their evolution (Kannan et al. 2014; Obreja et al. 2014), we have parametrized, in terms of the ratio $\mathrm{M_{star}/M_{halo}}$, a density profile that accounts for the effects of outflows in flattening the central dark matter distribution of haloes (Di Cintio et al. 2014b). This mass dependent profile is fully described in terms of the ratio $\mathrm{M_{star}/M_{halo}}$ and we will refer to it, throughout the paper, as the DC14 profile.

We aim to test whether such a mass dependent density profile is able to account for the kinematics of Local Group (LG) galaxies and whether this helps reconciling the "too big to fail" problem with abundance matching predictions. We use observed stellar velocity dispersions of LG galaxies from Kirby et al. (2014), which provide an estimate of the mass $\mathrm{M}(r_{1/2})$ (or equivalently of the circular velocity $\mathrm{V}(r_{1/2})$) enclosed within the galaxy's half-light radius $r_{1/2}$, and fit such data with theoretical rotation curves, in order to find the best fit halo mass for each galaxy. To model the distribution of dark matter within haloes, we use both the mass dependent DC14 density profile and the common NFW one, and compare the results arising from these two models against abundance matching relations in the LG (Brook et al. 2014; Garrison-Kimmel et al. 2014b).

The study of galaxies and satellites in the LG has two advantages over studying satellite populations in the Milky Way or M31: firstly, there is an added independent mass constraint coming from the timing argument (Kahn & Woltjer 1959; Li & White 2008); secondly, the mass function approaches a power law for all but the 10 most massive galaxies (Brook et al. 2014), which alleviates the large cosmic variance in satellite mass functions of individual haloes of the mass of M31 and the Milky Way (e.g. Purcell & Zentner 2012). Nevertheless, cosmic variance remains an issue in matching haloes to luminous galaxies within the LG, primarily in the normalisation of the adopted power law. The LG mass is dominated by the combined mass of the M31 and the MW, which are not constrained to fit the extended power law that we adopt for the halo mass function. We do explore the effects of a low normalisation of the power law in section 3.4 but it is beyond the scope of this paper to test whether an even lower normalisation is possible, a task which requires a significant number of LG analogue volumes to be simulated. This issue, and the key question of the number of "too big to fail" haloes, was examined in detail in Garrison-Kimmel et al. (2014b), to which we refer the reader.

The paper proceeds as follows: we present the observational data, the halo mass function, the abundance matching relation and the mass dependent density profile in section 2. We then use the observed kinematics to find the best fit dark matter halo for each galaxy in section 3.1. We show the resultant relations between $\mathrm{M_{star}}$ and $\mathrm{M_{halo}}$ for the two different density profiles in section 3.2, comparing them to the expectations from abundance matching and number of "too big to fail" haloes in section 3.4. We discuss the implications of our findings in terms of star formation efficiency in the LG in section 3.5. We present the cusp/core space of LG galaxies in section 3.6, providing a framework for comparisons with observations. In section 4 we discuss how the NFW profile cannot satisfactorily explain the kinematics of the full population of LG galaxies when compared with abundance matching predictions, enhancing the "too big to fail" problem, and how these issues are instead solved once the mass dependent DC14 profile is considered. We finally discuss possible caveats and implications of our findings.

## 2 DATA AND METHODS

### 2.1 Strategy

Kinematic information of LG members, both satellites and isolated, are used to find the mass of the dark matter halo that best fits each observed galaxy. The mass of each halo, $\mathrm{M_{halo}}$, is defined as the mass of a sphere of radius $\mathrm{R_{vir}}$ containing $\Delta_{\mathrm{vir}}$ times the critical matter density of the Universe $\rho_{crit} = 3H^2/8\pi G$ at z=0, where $\Delta_{\mathrm{vir}} = 18\pi^2 + 82x - 39x^2$ (Bryan & Norman 1998) and $x = \Omega_m - 1$ at z=0 depends on the selected cosmology.

**Table 1.** The number of haloes more massive than $M_{halo}$=5, 7 or $10\times10^9 M_\odot$ expected in a LG volume $V_{LG}$, considering a power law halo mass function. The count is shown for different normalizations of the most massive halo considered.

| max $M_{halo}(10^{12}M_\odot)$ | 2.0 | 1.4 | 1.0 | 0.8 |
|---|---|---|---|---|
| $M_{norm}(10^{10}M_\odot)$ | 4.4 | 3.2 | 2.4 | 2.0 |
| $N(>5\times10^9M_\odot)$ | 103 | 75 | 56 | 47 |
| $N(>7\times10^9M_\odot)$ | 76 | 55 | 41 | 34 |
| $N(>10^{10}M_\odot)$ | 55 | 40 | 30 | 25 |

Two different density profiles are used for dark matter haloes, along with a cosmologically motivated power law halo mass function to derive the distribution of available halo masses to which LG galaxies are assigned.

### 2.2 Halo mass function in the Local Group

We consider a spherical LG volume, $V_{LG}$, of radius 1.8 Mpc centred on the Milky Way. Such LG is a large enough volume in order for its halo mass function to be well described by a single power law, for all but the ∼ten most massive haloes, as was shown explicitly in Brook et al. (2014) and also found in other simulations of LG volumes (e.g. Gottlöber et al. 2010; Garrison-Kimmel et al. 2014b; Sawala et al. 2015). We therefore use a single power law, with slope of $-0.89$, to create a distribution of haloes within the LG, as in Brook et al. (2014), with $M_{halo}=[M_{norm}/N(>M_{halo})]^{(1/0.89)}$ where N=0.5,1.5.... is the number of haloes bigger than a given mass and $M_{norm}$ indicates the normalization.

We choose the normalization such that the most massive halo, whether it represents the Milky Way or the Andromeda galaxy, has a virial mass of $M_{halo}=1.4\times10^{12}M_\odot$, consistent with mass estimates of the MW (Battaglia et al. 2008; Watkins et al. 2010; Kafle et al. 2012; Boylan-Kolchin et al. 2013), M31 (Corbelli et al. 2010) and within the values allowed by the timing argument (Kahn & Woltjer 1959; Li & White 2008). This results in a LG abundance matching which smoothly joins the large scale surveys $M_{star}$-$M_{halo}$ relations (Guo et al. 2010; Moster et al. 2010; Behroozi et al. 2013) in a region where the two volumes overlap, i.e. for $M_{star}>10^8M_\odot$ (see section 3.4).

With this normalization there are 55 dark matter haloes with mass $M_{halo}>7\times10^9M_\odot$ within $V_{LG}$, which is the mass above which all haloes should contain stars according to the threshold dictated by reionization (Bullock et al. 2000, 2001; Boylan-Kolchin et al. 2012) and also to recent hydro-simulations (Okamoto & Frenk 2009; Sawala et al. 2015). More conservatively, there are 40 haloes more massive than $M_{halo}>1.0\times10^{10}M_\odot$.

Choosing a different normalization for the most massive halo in the LG will produce different counts in the number of haloes more massive than the reionization limit mass, as in Table 1.

### 2.3 Abundance matching in the Local Group

The abundance matching technique constrains the relationship between the stellar mass and the halo mass of galaxies (Moster et al. 2010; Guo et al. 2010; Behroozi et al. 2013). The idea is to match the cumulative number of observed galaxies above a given stellar mass within a given volume, with the number of dark matter haloes within the same cosmologically simulated volume. Such technique is *independent* of the halo density profile. Abundance matching relations are generally complete down to a stellar mass of $M_{star}\sim10^8M_\odot$, corresponding to the lower limit of large scale surveys such as SDSS (Baldry et al. 2008) and GAMA (Baldry et al. 2012). Above this mass, there is relatively little difference in the abundance matching studies (Guo et al. 2010; Moster et al. 2010; Behroozi et al. 2013), and such differences are insignificant in terms of our study.

Two recent works have extended the abundance matching relation to lower masses using the observed stellar mass function of the LG (Brook et al. 2014; Garrison-Kimmel et al. 2014b). In Brook et al. (2014), it was shown that using the average halo mass function of simulated local groups, which is well described by a power law, implies a steep relation between $M_{star}$-$M_{halo}$ in the region $10^{6.5}\lesssim M_{star}/M_\odot\lesssim10^8$. The empirically extended relation found in Brook et al. (2014) matches well the extrapolated abundance matching relation of Guo et al. (2010) and the relation found in Kravtsov (2010) based on the Milky Way satellites. In Brook et al. (2014) abundance matching subhaloes are also included within the total halo population, using their peak maximum halo mass value prior to stripping.

The second study (Garrison-Kimmel et al. 2014b) choses a particular collisionless simulation of the LG which has a flatter-than-average halo mass function, allowing the use of a slightly flatter $M_{star}$-$M_{halo}$ relation when matching the LG stellar mass function. Nevertheless, the Garrison-Kimmel et al. (2014b) and Brook et al. (2014) studies are compatible in the mass range $10^{6.5}\lesssim M_{star}/M_\odot\lesssim10^8$ to a similar degree as the various abundance matching relations in the mass range $M_{halo}\gtrsim10^8M_{star}$ (Moster et al. 2010; Guo et al. 2010; Behroozi et al. 2013; Moster et al. 2013).

The empirically extended relation found in Brook et al. (2014) and Garrison-Kimmel et al. (2014b) implies that galaxies with $10^{6.5}\lesssim M_{star}/M_\odot\lesssim10^8$ will all be housed within a narrow halo mass range, $10^{10}\lesssim M_{halo}/M_\odot\lesssim10^{10.5}$.

One assumption behind abundance matching is that every halo contains a galaxy; this may not be true for the smallest haloes, in which reionization may prevent the collapse of gas and subsequent star formation, leaving dark some haloes with $M_{halo}\lesssim10^9M_\odot$ (Bullock et al. 2000; Somerville 2002). A correction to the abundance matching relation has been proposed, taking into account this effect, by Sawala et al. (2015): by matching galaxies only to some of the smallest haloes, the relation between stellar mass and halo mass becomes flatter. This *adjusted* abundance matching starts deviating from the usual ones at about $M_{halo}<10^{10}M_\odot$. We emphasize that the LG abundance matching shown in Brook et al. (2014) and Garrison-Kimmel et al. (2014b) deals with a regime where *all* haloes are massive enough to be hosts of observed galaxies, therefore no correction is expected in this range where $M_{star}\gtrsim10^{6.5}M_\odot$ and $M_{halo}\gtrsim10^{10}M_\odot$.

Another factor that is often overlooked is the need to account for the baryon fraction $f_b$. Once abundance matching techniques are used to determine the expected mass of the dark matter halo of each galaxy, the actual mass of dark matter expected within the observed galaxy is only $(1\text{-}f_b)\sim0.83$ of that dark matter halo mass. We account for this in our study when comparing kinematically derived halo masses with dark matter haloes expected from abundance matching techniques. Finally, Sawala et al. (2015) also suggest that a further adjustment should be made, as they find that halo masses in hydrodynamical simulations can be up to 30% lower than in dark matter only simulations, i.e. a greater discrepancy than merely accounting for the baryon fraction $f_b$. We will discuss the consequences of such a reduction in halo mass on our results.

### 2.4 The observational dataset

We use the luminosities of LG galaxies, together with their luminosity-weighted average velocity dispersion and half-light radii, as compiled in Kirby et al. (2014). The data refer to galaxies with $10^5 \lesssim L_V/L_\odot \lesssim 2\times10^8$. Luminosities are converted to stellar masses following Woo et al. (2008) and Collins et al. (2014). From the Kirby et al. (2014) data set, we follow Tollerud et al. (2014) in excluding NGC 147 and NGC 185, whose relatively large baryonic mass and irregular kinematics make estimates of the dark matter profile highly uncertain, and follow Garrison-Kimmel et al. (2014a) in excluding NGC 6822 for similar reasons. We have instead added the Sagittarius dwarf irregular galaxy, which has well studied kinematics (Côté et al. 2000) and adds an extra isolated galaxy to our sample. This gives us a sample of 40 dwarf galaxies for which we have de-projected half-light radii $r_{1/2}$ and dynamical masses within such radii, $\mathrm{M}(r_{1/2})$.

It has been shown that stellar velocity dispersions can well constrain the dynamical masses of non-rotating, dispersion supported galaxies at $r_{1/2}$ (Wolf et al. 2010; Walker et al. 2009), minimizing the errors introduced by uncertainties of the anisotropy parameter. The mass within the half-light radius of such galaxies reads $\mathrm{M}(r_{1/2}) = 3\langle\sigma^2\rangle r_{1/2}/G$, where $\langle\sigma^2\rangle$ is the luminosity-weighted average of $\sigma^2$ over the whole galaxy (Wolf et al. 2010). The circular velocity is then $\mathrm{V}(r_{1/2}) = \sqrt{3\langle\sigma^2\rangle}$. This methodology has been shown to work also in non-spherically symmetric systems (Thomas et al. 2011). Some galaxies show significant rotation (Pegasus, WLM, Tucana, and And II): for such galaxies a rotation-corrected velocity for mass estimation is used, that takes into account pressure as well as rotation support in the calculation of $\mathrm{M}(r_{1/2})$ (Kirby et al. 2014).

### 2.5 The mass dependent "DC14" density profile

To model haloes that are flattened by energetic feedback processes, we use the mass dependent DC14 density profile (Di Cintio et al. 2014b), in which galaxies with $10^{6.5} \lesssim \mathrm{M_{star}} \lesssim 10^{10}\mathrm{M_\odot}$ have flatter central densities than the NFW profile (Di Cintio et al. 2014a).

The balance between the gravitational potential energy of haloes and the energy from the central star forming regions results in a maximum *core formation efficiency* found at $\mathrm{M_{star}} \sim 3\times10^8\mathrm{M_\odot}$, or equivalently $\mathrm{M_{star}/M_{halo}} \sim 0.004$ (Di Cintio et al. 2014a, Brook & Di Cintio 2015 in prep): steeper profiles form in lower mass dwarfs and higher mass galaxies. For low mass dwarfs, the halo maintains the NFW profile because there is not enough energy from supernovae driven outflows to flatten the dark matter cusp, while for high mass galaxies the inner density goes back toward a steep profile because the potential well of the increasingly massive halo is too deep for supernovae feedback to have an effect.

The DC14 profile has been derived using hydrodynamical cosmological simulations (Brook et al. 2012; Stinson et al. 2013) and accounts for the expansion of dark matter haloes as a response to the rapidly changing potential at the center of the galaxy due to the effects of feedback from baryons, particularly due to gas outflows generated in high density star forming regions. It takes the form (Merritt et al. 2006):

$$\rho(r) = \frac{\rho_s}{\left(\frac{r}{r_s}\right)^\gamma \left[1+\left(\frac{r}{r_s}\right)^\alpha\right]^{(\beta-\gamma)/\alpha}} \tag{1}$$

with the two free parameters being the scale radius $r_s$ and the characteristic density $\rho_s$. The remaining three parameters $(\alpha, \beta, \gamma)$, indicating the sharpness of the transition, the outer and the inner slope, respectively, are fully constrained via the stellar-to-halo mass ratio of a given galaxy, following Di Cintio et al. (2014b):

$$\begin{aligned}
\alpha &= 2.94 - \log_{10}[(10^{X+2.33})^{-1.08} + (10^{X+2.33})^{2.29}] \\
\beta &= 4.23 + 1.34X + 0.26X^2 \\
\gamma &= -0.06 + \log_{10}[(10^{X+2.56})^{-0.68} + (10^{X+2.56})]
\end{aligned} \tag{2}$$

where $X = \log_{10}(\mathrm{M_{star}/M_{halo}})$.

The DC14 profile thus has a range of inner slopes, dependent on the ratio $\mathrm{M_{star}/M_{halo}}$. The scale radius, $r_s$, is connected to the concentration of the halo, defined as $C = R_{\rm vir}/r_s$. Such concentration varies with respect to the N-body simulation case (Di Cintio et al. 2014b), once $r_s$ has been defined in terms of $r_2$ like in the NFW model:

$$C_{\rm DC14} = (1.0 + 0.00003e^{3.4X}) \times C_{\rm NFW} \tag{3}$$

where $X = \log_{10}(\mathrm{M_{star}/M_{halo}}) + 4.5$.

### 2.6 Setting Concentrations

For the NFW profile we tie concentrations to halo masses using the concentration-mass ($C-M$) relation derived within a Planck cosmology (Dutton & Macciò 2014). For the DC14 profile, we additionally use Eq. (3) to get the concentration of DC14 haloes once the concentration of NFW haloes has been set. In practice, since we are only dealing with dwarf and intermediate mass galaxies in this study, the two concentrations $C_{\rm DC14}$ and $C_{\rm NFW}$ are the same. Of course, scatter in the $C-M$ relation means that individual galaxies may live in more or less concentrated haloes than average. This reasoning, however, cannot be applied to the full set of LG galaxies, as it would be statistically challenging to assume that all of the LG galaxies live in underdense (or overdense) haloes. On average, we do expect that the 40 galaxies studied here should match the concentration-mass relation, with any scatter not affecting the final trends and conclusions of this work. We acknowledge that satellites are expected to live in haloes which are, on average, more concentrated than isolated ones; we verified that this effect is small (Dooley et al. 2014; Garrison-Kimmel et al. 2014a) and that it does not influence the results of this study.

Once a density profile and a concentration are set, the halo mass $\mathrm{M_{halo}}$ is the only free parameter left, since $(\alpha,\beta,\gamma)$ in the DC14 profile are constrained by the value of $\mathrm{M_{star}/M_{halo}}$ of each galaxy. The assumption that galaxies should follow the empirical mass-concentation relation is central to this study and to the "too big to fail" problem, since halo masses are not well constrained if the concentration is allowed to be a free parameter.

## 3 RESULTS

### 3.1 Assigning Local Group galaxies to haloes

We find the $\mathrm{M_{halo}}$ that provides the best fit to the observed velocity dispersion of each galaxy in our sample, in terms of circular velocity at the half-light radius, $\mathrm{V}(r_{1/2}) = \sqrt{3\sigma^2}$. $\mathrm{M_{halo}}$ values are drawn from the available dark matter haloes of the adopted LG halo mass function.

In the process of fitting, we are assuming that the inner region of each galaxy, at its half-light radius, has a density profile that is related to the mass of the halo prior to any tidal stripping from the

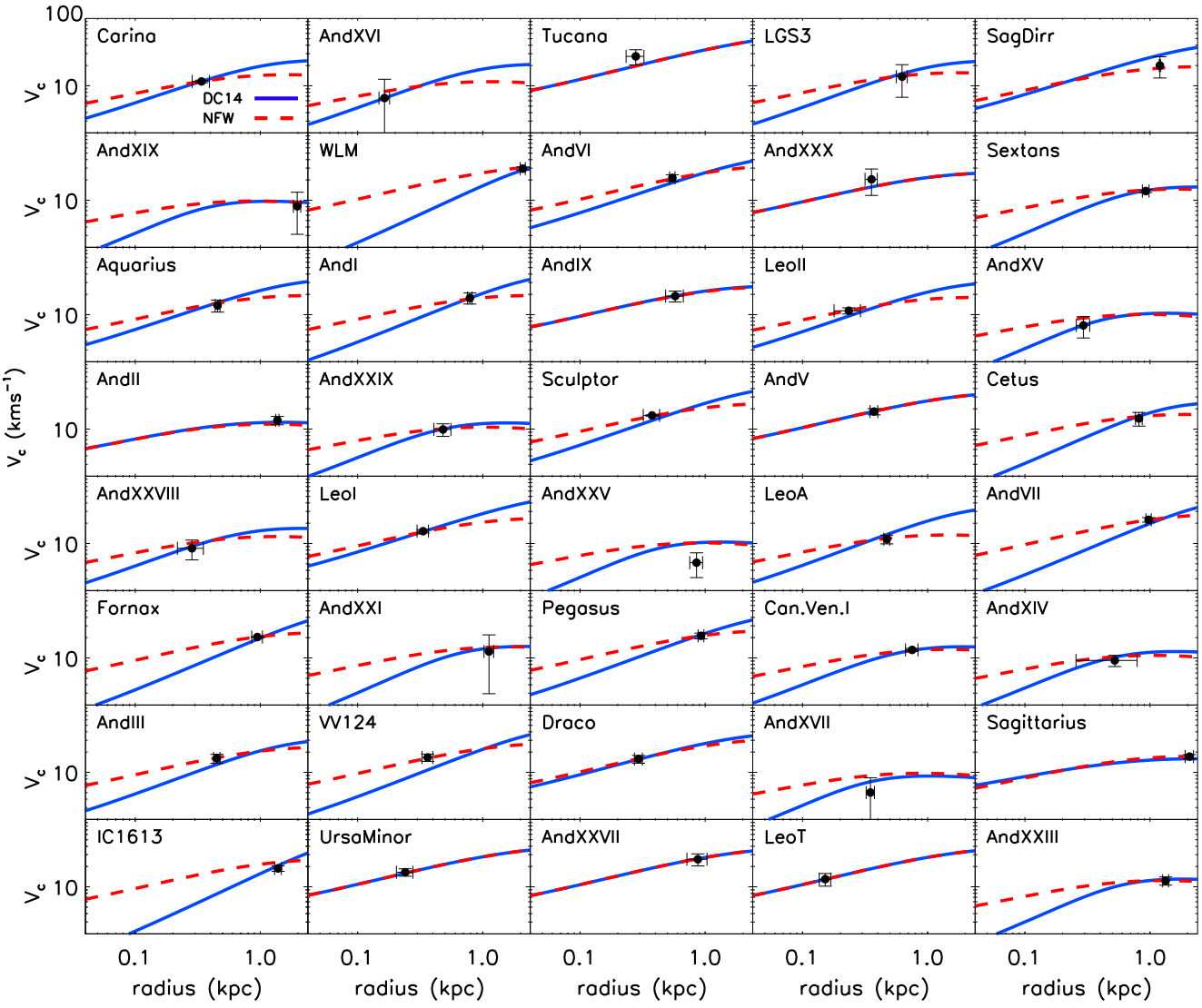


**Figure 1.** The rotation curves of LG galaxies, assuming an NFW (dashed red) or a DC14 (solid blue) density profile. The black points with error bars are observational data representing the circular velocities $V(r_{1/2})$, or equivalently the dynamical masses $M(r_{1/2})$, of galaxies within their half-light radii.

outer regions. Although satellite and isolated galaxies have undergone though different environmental processes, this is an appropriate assumption, given that the half-light radius of most of the galaxies studied is well within 1 kpc. The $M_{\rm halo}$ obtained by performing fits to the observed velocity dispersion should therefore be seen as halo masses prior to satellite's infall. [1]

The ten most massive galaxies of the LG, namely MW, M31, M33, LMC, NGC55, SMC, NGC205, M32, IC10 and NGC3109, are assumed to be housed within the ten most massive haloes available, a reasonable assumption given their kinematics and rotation curves. Therefore the ten most massive $M_{\rm halo}$ are not available to host the 40 galaxies studied in this work.[2]

The rotation curves of the best fit halo masses for each galaxy are shown in Figure 1, as red dashed lines when assuming an NFW density profile and blue solid lines for the DC14 model. Observational data, $V(r_{1/2}) = \sqrt{3\sigma^2}$, are shown as black points with error bars and are plotted versus half-light radius. Over the entire

[1] If, however, a satellite galaxy shows signs of tidal disruption or strong tidal interaction, it is not possible to exclude a priori that the inner region of such galaxy has been affected as well: in such case our methods returns a $M_{\rm halo}$ which is not necessarily representative of the unstripped, prior-to-infall halo mass. See Section 3.3 and 3.5 for further discussions.

[2] Any scatter in how we assign the 10 galaxies with highest stellar mass to the 10 most massive haloes does not affect our results, so long as these 10 objects are fit within haloes that are above the mass where reionization may cause some haloes to be dark.

population, the fitted velocity curves provide a reasonable agreement with the kinematics of observed galaxies, within the observational errors (apart from AndXXV, whose large half-light radius and low velocity dispersion indicates that it lives in a halo smaller than $M_{halo} \sim 10^8 M_\odot$ regardless of the profile used, which is the smallest halo considered available; we will come back on AndXXV in Section 3.6).

In Table 2 we list galaxies stellar masses and derived halo masses from our fits, for the NFW profile and the DC14 profile, respectively. For the DC14 profile, we also show the returned values of the transition parameter, outer and inner slopes, ($\alpha$,$\beta$,$\gamma$), corresponding to the best fit haloes. We note that the halo masses recovered in the NFW case are broadly consistent with the halo masses of LG galaxies found in the literature when assuming this profile, i.e. between $10^8$ and $10^9$ $M_\odot$ (e.g. Peñarrubia et al. 2008; Walker et al. 2009; Garrison-Kimmel et al. 2014a).

While more sophisticated mass modeling techniques have certainly been applied to some of the LG galaxies (e.g. Battaglia et al. 2008; Peñarrubia et al. 2008; Walker et al. 2009; Breddels & Helmi 2013, and references therein), we note that little consensus has been reached so far on the inner slope of dark matter haloes of individual members. Indeed, even the best data seem to be unable to distinguish between cores and cusps in dwarf galaxies (see for example Battaglia et al. 2008; Walker & Peñarrubia 2011; Strigari et al. 2014). Moreover, dynamical Jeans analysis of the radial velocity dispersion profiles of dSphs suffer from the well-known mass-anisotropy degeneracy, which makes difficult to assert the best halo mass value of such galaxies without the knowledge of their anisotropy parameter.

In our study we take another approach, comparing the effects of different density profiles on the population of LG galaxies *as a whole*, using the same method for all galaxies: we will see that specific trends become clear when comparing the resulting $M_{halo}$ obtained by using NFW versus DC14 profiles, even without using more sophisticated mass models.

Relative to the large range in mass that our sample explores, errors in the mass of individual galaxies are small, allowing us to interpret the trends seen in our ensemble. As mentioned in Section 2.6, the advantage of using a full statistical sample of galaxies is that the concentration-mass relation should apply and hold on average, excluding the possibility that all members live in particularly low concentration or low mass haloes as compared with theoretical expectations.

### 3.2 $M_{star}$-$M_{halo}$ relations for NFW and DC14 profiles

In Figure 2 we compare results for the ensemble of LG galaxies obtained by assuming either an NFW profile (left panel) or a DC14 one (right panel). The green vertical lines are the 55 dark matter haloes, from our halo mass function, with $M_{halo} > 7\times10^9 M_\odot$: they represent the "too big to fail" haloes, as in this region we expect all haloes to have stars.

The $M_{halo}$ values from our fits are shown as diamonds and plotted versus the $M_{star}$ of each galaxy. Black diamonds are satellite galaxies of the Milky Way and Andromeda galaxy, while magenta diamonds are isolated galaxies. Sagittarius dwarf spheroidal is indicated in cyan, as its stellar mass and kinematics (and therefore derived halo mass) have been significantly affected by its tidal disruption. We have accounted for the 17% reduction in halo mass due to the universal baryon fraction $f_b$ when comparing with abundance matching expectations from collisionless simulations, by actually plotting $M_{halo}/(1\text{-}f_b)$, where $M_{halo}$ is the halo mass derived from the kinematic fits.

Several abundance matching relations are superimposed on the plot (Guo et al. 2010; Brook et al. 2014; Garrison-Kimmel et al. 2014b; Sawala et al. 2015). As stated in Section 2.2, when using the fiducial LG mass normalization of $\max(M_{halo})=1.4\times10^{12} M_\odot$, the most massive galaxies (not subject of this study, and indicated as open squares) lie on the $M_{star}$-$M_{halo}$ plane in a way that joins nicely the abundance matching relations constrained by large scale surveys (Guo et al. 2010). The horizontal dotted line shows the approximate observational completeness limit of the LG, within a sphere of $\sim$ 1.8 Mpc of radius from the Milky Way: the census

**Table 2.** Compilation of galaxies used in this work. The observational stellar mass and the corresponding halo mass derived by fitting kinematical data using the NFW or the DC14 profile are listed for each galaxy, together with the $(\alpha, \beta, \gamma)$ parameters of the mass dependent profile. Satellite galaxies marked with a † do not follow the trends of isolated galaxies, which we interpret as indicating that environmental effects have occurred. In this case both the NFW and the DC14 profile fits would not return the halo infall mass: the quoted values of parameters for the DC14 case may not be valid.

| Galaxy Name | $M_{star}$ ($10^6 M_\odot$) | $M_{halo}$ ($10^8 M_\odot$) NFW | DC14 | $\alpha$ | $\beta$ | $\gamma$ |
|---|---|---|---|---|---|---|
| IC1613 | 102 | 24.4 | 447 | 2.57 | 2.50 | 0.233 |
| WLM | 44.7 | 60.2 | 158 | 2.63 | 2.50 | 0.244 |
| Sagittarius† | 26.9 | 7.00 | 7.00 | 0.854 | 2.85 | 1.09 |
| Fornax | 24.5 | 20.0 | 368 | 2.02 | 2.60 | 0.393 |
| AndVII | 14.8 | 30.2 | 223 | 2.02 | 2.60 | 0.394 |
| VV124 | 10.0 | 29.9 | 237 | 1.81 | 2.67 | 0.507 |
| AndII† | 9.55 | 2.00 | 4.00 | 1.33 | 2.74 | 0.894 |
| AndI | 7.59 | 10.0 | 146 | 1.91 | 2.63 | 0.453 |
| Pegasus | 6.61 | 25.0 | 200 | 1.70 | 2.72 | 0.573 |
| LeoI | 4.90 | 19.9 | 289 | 1.38 | 2.87 | 0.761 |
| AndVI | 3.98 | 59.2 | 190 | 1.48 | 2.82 | 0.700 |
| Sculptor | 3.89 | 20.2 | 152 | 1.58 | 2.77 | 0.643 |
| Cetus | 3.16 | 6.01 | 29.9 | 2.24 | 2.54 | 0.299 |
| LeoA | 2.95 | 3.00 | 80.1 | 1.75 | 2.69 | 0.544 |
| SagDirr | 2.29 | 9.95 | 140 | 1.37 | 2.88 | 0.771 |
| AndIII | 1.82 | 19.8 | 50.2 | 1.74 | 2.70 | 0.548 |
| Aquarius | 1.41 | 9.98 | 61.3 | 1.53 | 2.80 | 0.674 |
| AndXXIII† | 1.26 | 2.30 | 3.99 | 2.65 | 2.50 | 0.255 |
| LeoII | 1.17 | 8.01 | 70.3 | 1.38 | 2.88 | 0.765 |
| AndXXI† | 1.02 | 4.01 | 6.01 | 2.45 | 2.51 | 0.241 |
| Tucana | 0.933 | 404 | 404 | 1.00 | 3.00 | 1.00 |
| Draco | 0.912 | 50.2 | 88.2 | 1.15 | 3.02 | 0.904 |
| Sextans† | 0.851 | 4.00 | 7.02 | 2.30 | 2.53 | 0.278 |
| LGS3 | 0.724 | 5.00 | 19.9 | 1.74 | 2.70 | 0.547 |
| AndXXV† | 0.676 | 1.20 | 2.00 | 2.66 | 2.51 | 0.263 |
| AndXV† | 0.631 | 1.15 | 2.00 | 2.65 | 2.50 | 0.255 |
| AndXIX† | 0.575 | 1.02 | 1.50 | 2.67 | 2.51 | 0.283 |
| UrsaMinor | 0.562 | 101 | 101 | 1.00 | 3.00 | 1.00 |
| AndXVI | 0.525 | 1.80 | 14.0 | 1.76 | 2.69 | 0.538 |
| Carina | 0.513 | 3.99 | 20.0 | 1.58 | 2.77 | 0.644 |
| AndV | 0.398 | 70.3 | 68.8 | 1.00 | 3.00 | 1.00 |
| AndXXVII† | 0.363 | 88.2 | 92.9 | 1.00 | 3.00 | 1.00 |
| AndXVII | 0.309 | 1.01 | 1.14 | 2.62 | 2.50 | 0.241 |
| Can.Ven.I† | 0.309 | 3.00 | 5.00 | 1.99 | 2.61 | 0.411 |
| AndXIV† | 0.302 | 1.50 | 3.20 | 2.19 | 2.56 | 0.320 |
| AndXXVIII† | 0.275 | 2.50 | 6.98 | 1.78 | 2.68 | 0.525 |
| AndXXIX† | 0.234 | 1.40 | 3.00 | 2.10 | 2.58 | 0.358 |
| AndIX | 0.200 | 26.8 | 25.5 | 1.02 | 3.11 | 0.985 |
| LeoT | 0.182 | 90.5 | 90.5 | 1.00 | 3.00 | 1.00 |
| AndXXX | 0.170 | 25.3 | 25.3 | 1.00 | 3.00 | 1.00 |

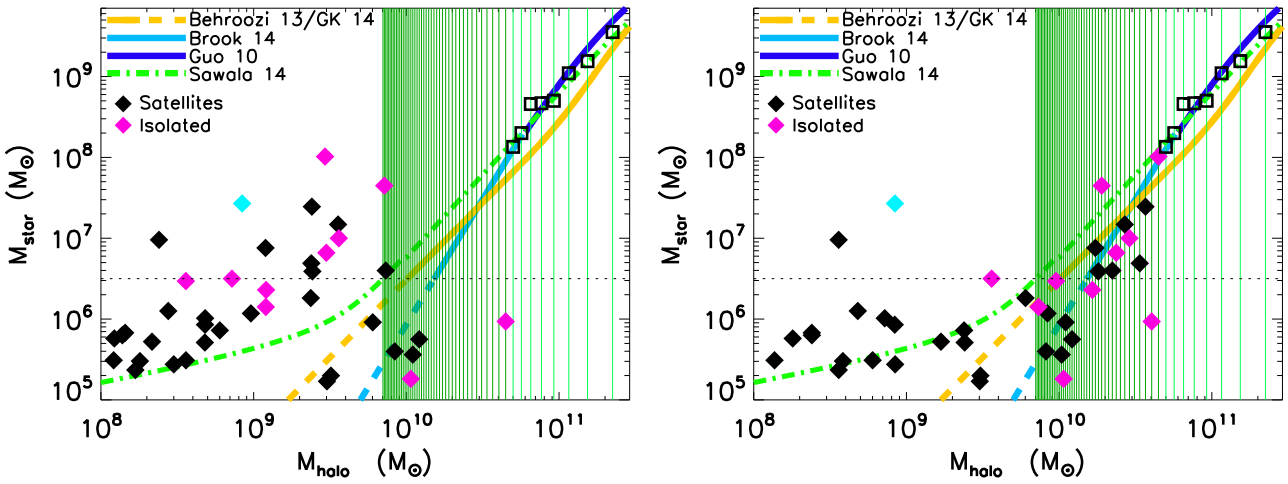


**Figure 2.** The relation between observed stellar mass and derived halo mass for LG galaxies. The halo mass has been found by fitting kinematical data and assuming two different halo profiles. The results for an NFW profile are shown in the left panel, while the mass dependent DC14 halo profile has been used in the right panel. Satellites and isolated galaxies are shown in different colors, with Sagittarius dwarf irregular, highly affected by tides, shown in cyan. Several abundance matching predictions are indicated, in particular the Brook et al. (2014) one has been constrained using the LG mass function, and it is shown as dashed line below the observational completeness limit of the LG.

of galaxies with stellar masses lower than $\sim$3-5$\times10^6$M$_\odot$ is likely incomplete in this volume (Tollerud et al. 2008).

The difference between the two derived M$_{\rm star}$-M$_{\rm halo}$ distributions is striking. For the NFW profile, the observed kinematics imply that the galaxies are well fit by haloes with masses $10^8\lesssim$M$_{\rm halo}$/M$_\odot\lesssim10^{10}$: only one galaxy from our sample fits to a halo which is more massive than $10^{10}$M$_\odot$, in disagreement with abundance matching predictions (Brook et al. 2014). Using the NFW profile to describe the kinematics of LG members highlights the "too big to fail" problem in the LG (Garrison-Kimmel et al. 2014a; Kirby et al. 2014): almost none of the most massive haloes, indicated as vertical green lines, has been assigned to a galaxy. The *darkness* of the haloes with mass M$_{\rm halo}>7\times10^9$M$_\odot$ can not be explained simply by invoking reionization processes, as these haloes are more massive than the reionization mass threshold (Boylan-Kolchin et al. 2012).

The preferred values of M$_{\rm halo}$ resulting from an NFW model are in disagreement with abundance matching relations even after taking into account the reduction of dark matter mass by up to a 30% caused by baryonic effects and the fact that some of the smallest haloes remain dark (Sawala et al. 2015).

A different picture appears for the DC14 profile, shown in the right panel of Figure 2. Now the most massive dwarfs, those with M$_{\rm star}\gtrsim3-5\times10^6$ M$_\odot$, all fit in haloes more massive than M$_{\rm halo}\sim10^{10}$M$_\odot$ (apart from two outliers far from equilibrium, namely Sagittarius dSph, which is being disrupted, and AndII, which shows signs of a merger, Amorisco et al. 2014a): the distribution of preferred halo masses is therefore shifted toward the right side of the plot. This can be easily understood in terms of halo profiles: galaxies with a M$_{\rm star}$/M$_{\rm halo}$ ratio higher than 0.0001 develop the minimum amount of energy, from stellar feedback, required for their profile to be shallower than NFW. In this way a galaxy like Fornax, for example, with M$_{\rm star}\sim2\times10^7$M$_\odot$, will be well fit by an NFW halo with M$_{\rm halo}\sim2\times10^9$M$_\odot$ or by a more massive DC14 halo with M$_{\rm halo}\sim3\times10^{10}$M$_\odot$ and inner slope $\gamma\sim-0.39$.

Moving the distribution of M$_{\rm star}$-M$_{\rm halo}$ to the right has two consequences: firstly, the number of "too big to fail" haloes is considerably reduced, as we are assigning galaxies to haloes more massive than M$_{\rm halo}\sim7\times10^9$M$_\odot$; secondly, the distribution is now in agreement with the abundance matching predictions of Brook et al. (2014) and Garrison-Kimmel et al. (2014b), down to the observational completeness limit of the LG.

Below the completeness limit of M$_{\rm star}\sim3-5\times10^6$ M$_\odot$, many galaxies still prefer to live within less massive haloes than an *extrapolation* of abundance matching would predict, even when applying the DC14 profile. A comparison with the proposed abundance matching of Sawala et al. (2015) seems to provide a good agreement with the kinematic of such low mass galaxies, when the DC14 profile is assumed.

However, all the dwarf galaxies in this low halo mass region are satellites of either the Milky Way or Andromeda: the fact that no isolated galaxy is found within such low mass haloes, M$_{\rm halo}\lesssim3\times10^9$ M$_\odot$, suggests that environmental effects are in place. Indeed, for most of the satellites in this region, signs of tidal interaction have been invoked in the literature (Okamoto et al. 2012; Battaglia et al. 2011, 2012), and we will name and discuss these objects in section 3.3. Numerical simulations suggest that environmental effects may be important even in the inner region of galaxies once baryonic physics have been taken into account, since the presence of a baryonic disk can enhances tidal effects (Brooks & Zolotov 2014; Arraki et al. 2014). Tidal effects are even more important in those satellites that formed a core at early times, before infall into the main host (Peñarrubia et al. 2010; Zolotov et al. 2012; Madau et al. 2014). Tides are therefore a possible mechanism to reduce the masses of such galaxies (Collins et al. 2014).

Our analysis therefore supports the notion that a combination of dark matter halo expansion due to baryonic effects and enhanced environmental processes can explain the kinematics of LG galaxies. Satellite galaxies living in the low halo mass region have likely been placed there because their kinematic has been affected by tides, and they would have had a higher halo mass otherwise (Collins et al. 2014), bringing them in agreement with the Brook et al. (2014) and Garrison-Kimmel et al. (2014b) abundance matching (and their extrapolation). On the other side, all the isolated galaxies match such relations when the DC14 model is assumed.

### 3.3 Environmental Effects?

To test further the notion that environmental effects may play a role in determining the kinematics of satellite galaxies that are assigned to low mass haloes, we show the galaxies in the plane of $M_{star}$ versus inner slope $\gamma$ in the top panel of Fig 3, where satellite galaxies are indicated in black and isolated objects in magenta. Galaxies whose best fit halo is less than $10^9 M_\odot$ in the DC14 case, are marked with red circles, and it is evident how they do not follow the same relation of increasingly cored profile for increasing stellar mass followed instead by isolated galaxies. The trend of lower $\gamma$ for higher $M_{star}$ is in very good agreement with previous results from Zolotov et al. (2012) who studied satellite galaxies within hydrodynamical simulations.

We then plot, in the lower panel of Fig 3, the half-light radius $r_{half}$ versus stellar mass of LG galaxies. The satellites that we have interpreted as being environmentally affected are again marked with red circles; they tend to have larger $r_{half}$ values at given $M_{star}$, compared to the isolated sample, as expected if tidally effects have been in place. If environmental effects have influenced this subsample of satellite galaxies, then we emphasise that both the NFW and the DC14 profile would not return the satellite halo mass at its peak, i.e. at infall time, as it would be desirable, but rather the z=0 halo mass. This would invalidate the values given in Table 3.1 for these satellite galaxies, which we indicate with a †. In particular, the inner slopes shown for those particular satellite galaxies should not be considered a prediction of this study. Indeed the DC14 density profile, parametrized as a function of $M_{star}/M_{halo}$, accounts for the impact of outflows of gas within galaxies but has not been designed to include tidal effects.

It is possible however that cores have formed in some of these satellite galaxies at earlier times, when the energetic requirement for core formation was lower given the lower halo mass (Peñarrubia et al. 2012; Amorisco et al. 2014a; Madau et al. 2014), and that such galaxies have further evolved and interacted with the main hosts, causing tides to play an important role in their dynamics (Arraki et al. 2014; Brooks & Zolotov 2014).

Two satellite galaxies appear in the upper, left region of Figure 2 . The first, Sagittarius dwarf spheroidal (Ibata et al. 1994), is currently interacting with the Milky Way's disk and has been severely stripped and disrupted; the second one, the Andromeda II satellite of M31, has been reported to be the remnant of a merger between two dwarf galaxies (Amorisco et al. 2014a), which may have had a strong impact on its kinematics.

Excluding Sagittarius, three Milky Way satellites are found not to lie on the abundance matching relation, namely Sextans, Carina and Canes Venatici I, with some of them living in a region where shallow profiles are preferred. The irregular, distorted shape of Canes Venatici I could indicate that it is suffering from tidal effects (Okamoto et al. 2012), although it is one of the most distant satellites of our Galaxy. It has been argued that the young stellar population of this galaxy, having a small velocity dispersion, could reflect the presence of a cored profile (Ibata et al. 2006). Sextans shows remarkable velocity gradients that could have been caused by its tidal disruption from the Milky Way (Battaglia et al. 2011) and its observed stellar clumps are in agreement with a cored dark matter halo (Lora et al. 2013).

Finally, Carina's spatial extent of member stars (Kuhn et al. 1996) and observed tidal debris (Battaglia et al. 2012) provide evidence of tidal interactions, although such tidal features have been recently found to be weaker than previously thought (McMonigal et al. 2014).

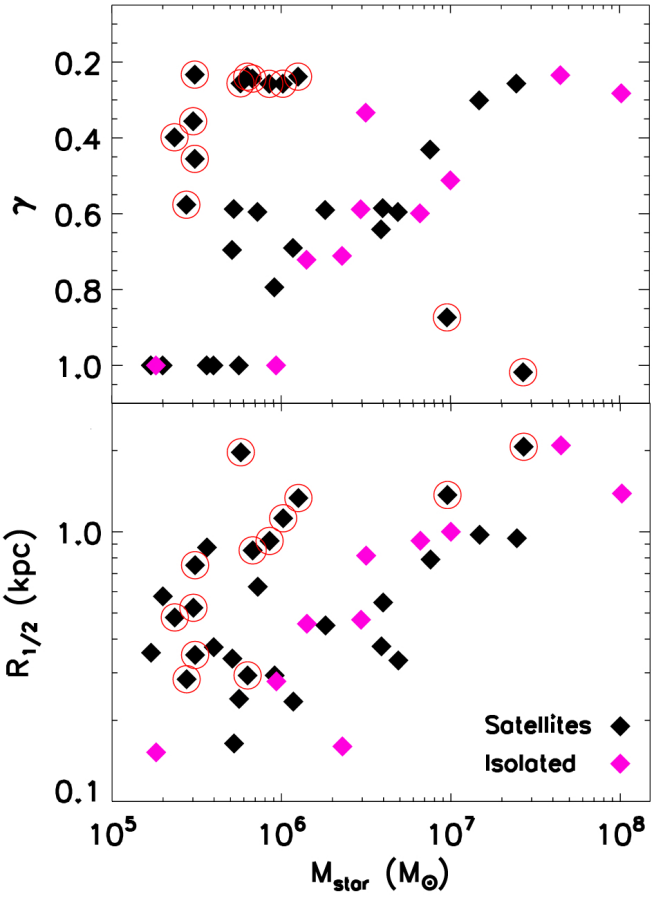


**Figure 3.** The upper panel shows the derived inner slope, $\gamma$ from DC14 profile, against $M_{star}$ for isolated (magenta) and satellite (black) LG galaxies. Satellites whose best fit halo mass is low compared to abundance matching expectations ($M_{halo}<10^9 M_\odot$) are marked with red circles: they do not follow the same trend of decreasing $\gamma$ (cored profile) for increasing $M_{star}$ as isolated galaxies. The lower panel shows the half-light radii versus $M_{star}$, using the same symbols. The satellites living in low halo masses have relatively high half-light radii compared to the isolated galaxies of similar $M_{star}$, a further indication that they may have been tidally affected.

The remaining galaxies which prefer to live in haloes smaller than $M_{halo}\sim 3\times10^9 M_\odot$ are satellite galaxies of Andromeda. AndXIV, AndXV, AndXVI, AndXIX, AndXXI and AndXXV are extreme outliers, given their high half-light radius and low velocity dispersion, and has been suggested (Collins et al. 2014) that tides may explain their associated low masses. Collins et al. (2014) points out that the fact that more Andromeda satellites fit to low mass haloes than Milky Way satellites do, may indicate that these systems have been, in general, more strongly affected by tides.

Moreover, the z=0 halo mass for AndXXV must be even lower than $M_{halo}\sim 10^8 M_\odot$, given that we could not fit its kinematic with any of the available haloes from our halo mass function, whose lowest considered halo is $M_{halo}\sim 10^8 M_\odot$: as pointed out in Collins et al. (2014), with such a low halo mass this galaxy should not have formed any stars, unless its mass was significantly higher in the past, prior to being accreted.

Support for the notion that satellites assigned to low mass halos by our model have been affected by the environment comes from the work of Zolotov et al. (2012), in which it was shown that satellites in hydrodynamical simulations may have their velocities reduced even in the inner 1kpc.

### 3.4 On the normalization of the Local Group mass

A degree of uncertainty exists in the mass estimates of the MW (Battaglia et al. 2008; Boylan-Kolchin et al. 2013; Watkins et al. 2010; Kafle et al. 2012, 2014, and references therein), M31 (e.g. Corbelli et al. 2010) and of the LG (Klypin et al. 2002; Li & White 2008; van der Marel et al. 2012; González et al. 2014; Peñarrubia et al. 2014; Diaz et al. 2014): we explore here how this affects our results. Our fiducial model assumes that the most massive galaxy, whether it is the MW or M31, has a mass of $M_{\rm halo}$=$1.4\times10^{12}M_\odot$, close to the most favored observationally determined values.

In Figure 4 we show the abundance matching relations that arise using such a fiducial maximum halo mass, as well as a normalization with maximum mass of $M_{\rm halo}$= $0.8\times10^{12}M_\odot$, which is around the lowest estimate of the Milky Way and Andromeda mass. We compare the results with large scale surveys abundance matching.

The red crosses are LG galaxies matched to corresponding haloes[3] for the fiducial model: such matching results in the already shown (Figure 2) slope of Brook et al. (2014), indicated as cyan solid line. Interestingly, when using this fiducial model, the highest mass LG galaxies are matched to haloes in such a way that the resulting relation between $M_{\rm star}$ and $M_{\rm halo}$ is in agreement with large volume abundance matchings (Guo et al. 2010; Behroozi et al. 2013, shown as dark blue and yellow line, respectively) in the mass region where the two different volumes overlap, and matches their extension to lower masses (Brook et al. 2014; Garrison-Kimmel et al. 2014b).

By contrast, choosing the lower mass normalization results in LG galaxies being assigned to systematically less massive haloes than found in abundance matching studies of large scale surveys (e.g. Guo et al. 2010; Moster et al. 2013), in a region where the two volumes overlap, as can be seen from the violet plus signs compared to the dark blue line in Figure 4. Moreover, a maximum halo mass as low as $M_{\rm halo}$= $0.8\times10^{12}M_\odot$, although allowed by current estimates of the MW and M31 mass (Battaglia et al. 2008; Kafle et al. 2014; Corbelli et al. 2010), will result in tension with the lowest LG mass estimates from timing arguments (Li & White 2008).

Nevertheless, to show that our main results are only marginally affected by the chosen normalization of the LG, in Figure 5 we repeat the analysis using the low mass normalization of the halo mass function, max($M_{\rm halo}$)=$0.8\times10^{12}M_\odot$. We remind that we fit kinematics of the sample of LG galaxies with the most appropriate halo drawn from this halo mass function. The best fit haloes when assuming the NFW profile (left panel) have almost not changed compared to the results shown in Figure 2. What has changed is the number of "too big to fail" haloes, shown as green lines, which we discuss below.

For the DC14 profile, a lack of availability of appropriate mass haloes from the halo mass function means that several of the highest mass galaxies are matched to haloes with lower mass than was the case in Figure 5, meaning haloes with lower mass than their kinematic fits warrant. One way to look at this is that the amount of expansion predicted in the DC14 profile matches the kinematics of the LG galaxies for the fiducial normalization, but a lower normalization would be best fit by models with slightly less halo expansion. Regardless, the main differences between the NFW and DC14 distributions are retained, confirming our finding that expanded haloes are needed to match abundance matching predictions in the LG.

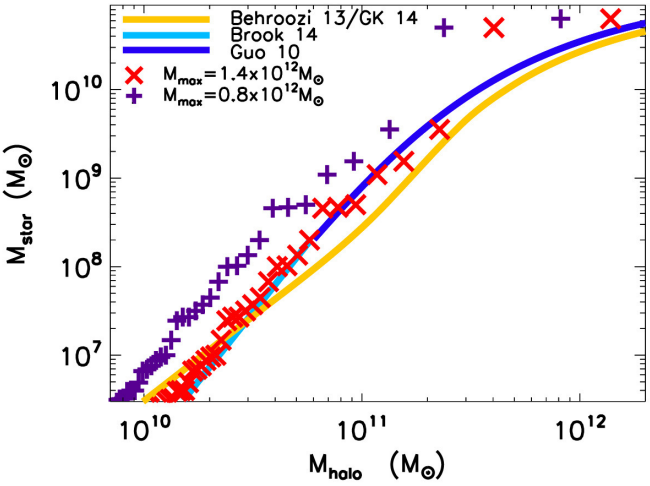


**Figure 4.** The abundance matching in the LG, derived by ordering galaxies by stellar mass and matching them to a power law halo mass function with two different normalizations: a maximum halo mass of $M_{\rm halo}$=$1.4\times10^{12}M_\odot$(red crosses) or a lower maximum halo mass of $M_{\rm halo}$=$0.8\times10^{12}M_\odot$ (violet plus) have been used. The distribution of red crosses is equivalent to the Brook et al. (2014) slope, cyan line here and in Figure 2, which has indeed been derived using such fiducial maximum halo mass: in this case both the slope *and* the normalization of LG galaxies are in agreement with abundance matching results of large galaxy surveys (Guo et al. 2010; Behroozi et al. 2013). A lower normalization would instead result in the ensemble of LG galaxies being matched to systematically lower mass haloes than predicted from large surveys, which are well constrained for $M_{\rm star}\gtrsim10^8M_\odot$.

The degree to which the "too big to fail" is solved depends on the normalization of the LG. As from Table 1, there are 55 haloes more massive than $M_{\rm halo}\sim7\times10^9M_\odot$ for our fiducial normalization and 34 for the lowest mass normalization, shown as vertical green lines in Figure 2 and Figure 5, respectively. The completeness limit of the LG must be considered when counting the "too big to fail" haloes that have not been assigned to a galaxy, as uncertainties remain about the exact number of galaxies with $M_{\rm star}<3\times10^6M_\odot$, and some of them may be expected to match haloes with $M_{\rm halo}\gtrsim7\times10^9M_\odot$.

Considering therefore the completeness limit of LG surveys, for our fiducial normalization, there are $\sim$ 28 haloes more massive than $M_{\rm halo}\sim1.5\times10^{10}M_\odot$, i.e. above the point where the Brook et al. (2014) abundance matching in Figure 2 crosses the line where $M_{\rm star}=3\times10^6M_\odot$: 10 of such haloes are assigned to the LG galaxies studied here if a DC14 profile is used, and another 10 are expected to host the most massive LG members (MW, M31 etc., indicated as open squares in Figure 2). Asides from the 10 most massive galaxies, there are another 8 galaxies (NGC 185, NGC 147, IC 5152, Sextans B, Sextans A, And XXXI, And XXXII, UKS2323-326) within the completeness limit, i.e. with stellar masses $M_{\rm star}>3\times10^6M_\odot$, not included in our sample because their current kinematic information made it difficult to determine their halo masses. Assigning these 8 galaxies to the remain-

[3] We are in a region where all haloes are expected to host galaxies, therefore a one-to-one matching is appropriate.

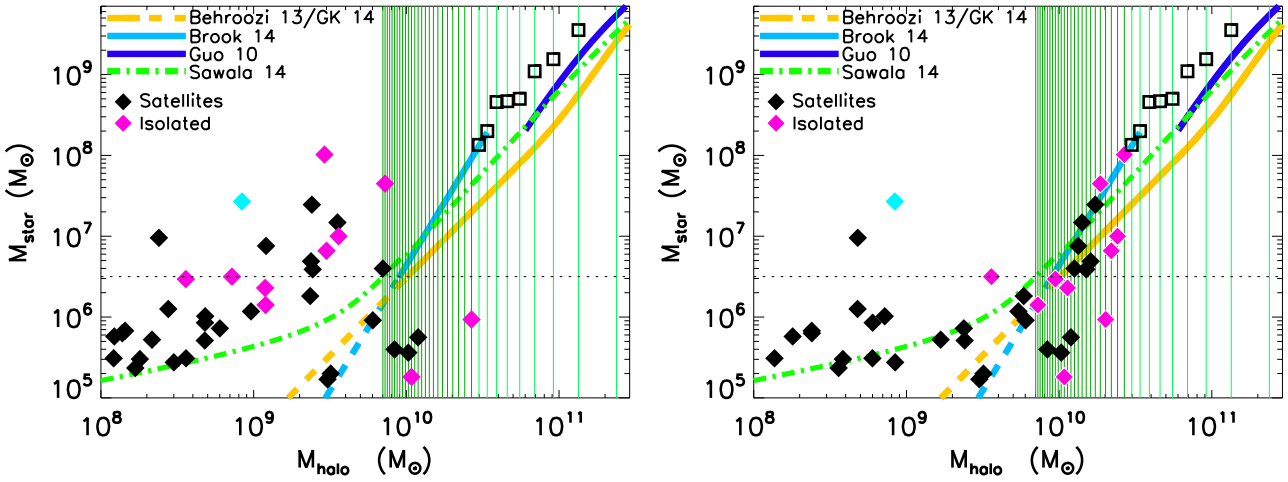


**Figure 5.** Same as in Figure 2, but for a lower normalization of the LG mass. The most massive galaxy in this case has a halo mass of $M_{halo}$=$0.8\times10^{12}M_\odot$, which correspond to the lowest mass estimates of MW and M31. The results for an NFW profile are shown in the left panel, while the mass dependent DC14 halo profile has been used in the right panel. Given the change in halo mass function normalization, the Brook et al. (2014) abundance matching has been shifted accordingly, and is equivalent to the distribution of violet plus signs of Figure 4.

ing 8 massive haloes would completely solve the "too big to fail" problem in a region where the census of LG galaxies is complete.[4]

The situation is different for an NFW profile, in which none of the studied LG galaxies is assigned to haloes more massive than $M_{halo}\sim 10^{10}M_\odot$, leaving $\sim$ 9 massive failures above the completeness limit of the LG.

Below the completeness limit, counting all the haloes more massive than $M_{halo}\sim 7\times10^9M_\odot$, the DC14 profile results in 17 haloes unaccounted for versus 30 in the NFW case. Recall, however, that several of the lowest mass ($M_{star}\lesssim 3\times10^6M_\odot$) satellite galaxies have likely been affected by environmental processes, so that their estimated halo mass is actually a lower limit of their virial mass: assuming that some of these galaxies have a mass higher than what suggested by their z=0 kinematics will further help in bringing the number of observed galaxies in agreement with theoretical predictions, once the DC14 profile is assumed.

Finally, we want to highlight the case of Tucana: it is an extremely low luminosity galaxy that fits nevertheless to a halo $M_{halo}\gtrsim 10^{10}M_\odot$, regardless of the density profile used. The census of LG galaxies within 1.8 Mpc of the Milky Way is complete only down to $M_{star}> 3-5\times10^6M_\odot$ (Koposov et al. 2008; Tollerud et al. 2008) and future deep surveys will hopefully increase the agreement between theoretical expectations and observations, if a few new faint galaxies with similarly high velocity dispersions as Tucana are discovered.

Using the lower normalization, as in Figure 5, will result in the abundance matching (now shifted to the left to reflect the average slope and normalization of the violet signs in Figure 4) to hit the observational completeness limit at $M_{halo}\sim 8.8\times10^9M_\odot$, with again 28 haloes more massive than this value. In the DC14 case, every halo more massive than $M_{halo}\sim 7\times10^9M_\odot$ (34 in total) has been assigned to a galaxy, while in the NFW case we are still left with 9 of such haloes not forming any stars, all of them lying in a region where the LG is observationally complete

[4] In the following discussion we assume that these 8 galaxies live into massive haloes, $M_{halo}\gtrsim 7\times10^9M_\odot$, for both the NFW and DC14 case.

### 3.5 Star formation efficiency in isolated Local Group galaxies

Abundance matching relations from large scale surveys have shown that the galaxy formation efficiency, $M_{star}/M_{halo}$, decreases sharply as $M_{halo}$ decreases for $M_{halo}\lesssim 10^{11.5}M_\odot$: below this mass the relation can be approximated by a power law, $M_{star}\sim M_{halo}{}^\alpha$, whose slope depends on the observed faint end of the luminosity function, leading to values of $\alpha\sim3$ (Guo et al. 2010) and $\alpha\sim2.4$ (Moster et al. 2013). LG abundance matching has shown that the relation extends to significantly lower stellar mass, $M_{star}\gtrsim10^{6.5}M_\odot$, providing values of $\alpha\sim3$ (Brook et al. 2014) and $\alpha\sim1.9$ (Garrison-Kimmel et al. 2014b). [5]

Although the variation between these results is not insignificant, they all indicate that $M_{star}$ decreases sharply as $M_{halo}$ decreases, i.e. the efficiency of a galaxy in converting baryons into stars decreases with decreasing $M_{halo}$, such that dwarf galaxies are the objects with the lowest star formation efficiency in the Universe.

An interesting aspect of our analysis is reported in Figure 6, in which the star formation efficiency, $M_{star}/M_{halo}$, is shown as a function of $M_{halo}$ for the isolated LG galaxies from our sample. Best fit halo masses are derived assuming an NFW profile (blue circles) or DC14 profile (magenta diamonds). The solid and dashed lines are predictions from different abundance matching relations. Regardless of LG mass, the NFW model places galaxies with $10^6\lesssim M_{star}/M_\odot\lesssim10^8$ within haloes of $10^8\lesssim M_{halo}/M_\odot\lesssim5\times10^9$, implying a reversal of the steep trend of decreasing star formation efficiency, also observed if the *adjusted* abundance matching (Sawala et al. 2015) is applied: several of these galaxies are assigned to such small haloes that their efficiency is comparable to the one of objects 2-3 orders of magnitude more massive.

A reversal of the trend is difficult to explain within our current theoretical framework of galaxy formation. Rather, one may expect

[5] Kravtsov (2010) infers a similar relation, with slope $\alpha$=2.5, from the MW satellite luminosity function. However, this estimate has larger uncertainties than the afore mentioned studies due to the less well constrained halo mass function of an individual MW dark matter halo, and due to the considered mass range in which some halo may be dark due to reionization.

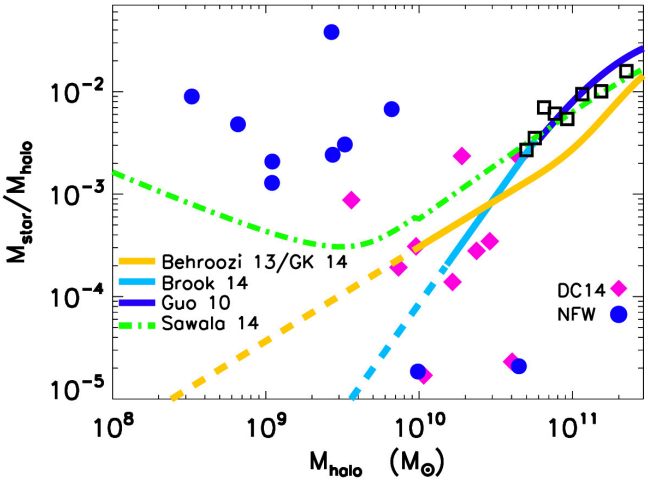


**Figure 6.** The galaxy formation efficiency, $M_{star}/M_{halo}$, as a function of $M_{halo}$ for isolated LG galaxies. The best fit halo mass has been derived using an NFW (blue circles) or a DC14 (magenta diamonds) profile. The solid and dashed lines represent different abundance matching prescriptions.

that at lower galaxy masses, the combined effects of feedback and reionization would further suppress star formation efficiency.

Indeed, in low-mass systems, both winds from supernovae (Oppenheimer & Davé 2008) and the presence of a UV background can further reduce the amount of gas that cools at the center of a halo (Navarro & Steinmetz 1997): reionization, in particular, completely prevents the formation of galaxies within several of the smallest haloes (Bullock et al. 2000). Hydrodynamical simulations have shown that the steep declining in $M_{star}/M_{halo}$ holds at low masses, with ultrafaint dwarfs of stellar masses $10^4 \leqslant M_{star}/M_\odot \leqslant 10^5$ expected to inhabit haloes of a few times in $10^9 M_\odot$ (Brook et al. 2012; Munshi et al. 2013; Shen et al. 2014; Hopkins et al. 2014). Semi-analytic models also predict that star formation efficiency will continue to decrease as halo mass decreases (Benson et al. 2002; Guo et al. 2011).

To explain the star formation efficiency of LG dwarf galaxies inferred using the NFW model, one would require a physical mechanism that leads such low mass haloes, $M_{halo} \lesssim 10^9 M_\odot$, to have the same efficiency, in terms of $M_{star}/M_{halo}$, as haloes with mass $M_{halo} \sim 10^{11} M_\odot$. This reasoning is specially important for isolated LG members, in which environmental effects can not be invoked to reduce their halo masses.

By contrast, when halo masses are derived assuming a DC14 profile, the efficiency of the isolated dwarfs matches the relation between $M_{star}/M_{halo}$ and $M_{halo}$ implied by the abundance matching of Brook et al. (2014), Garrison-Kimmel et al. (2014a) and their extrapolations below $M_{star} \sim 3 \times 10^6 M_\odot$, as well as current cosmological simulations. While some scatter is observed, and may be expected at such low halo masses due to the variety of star formations histories (Weisz et al. 2014) and merging histories of such systems, the average trend remains clearly a decline in $M_{star}/M_{halo}$ as we lower the halo mass, in agreement with both large scale and LG abundance matchings.

From another perspective, if one *assumes* that the slope of $M_{star}/M_{halo}$ as a function of $M_{halo}$ extends to the mass range of LG dwarf galaxies, one would *require* expanded haloes to explain the kinematics of such galaxies.

### 3.6 The cusp/core space of Local Group galaxies

The cusp/core transformation within galaxies is predicted to depend on the ratio of stellar-to-halo mass, and it is expected if $0.0001 \lesssim M_{star}/M_{halo} \lesssim 0.03$.

In Figure 7 we provide a different perspective of our findings, showing the $M_{star}$-$M_{halo}$ results from the right panel of Figure 2 imposed on the "cusp/core" space, colored by the value of the inner slope $\gamma$ according to the DC14 profile [6]. We have excluded the satellite galaxies that we believe may have been influenced by tides, those marked † in table 3.1, as the inner slope results may not be appropriate in such cases.

Galaxies are explicitly named and color coded according to their membership, with Milky Way's satellites in cyan, Andromeda's satellites in white and isolated galaxies in magenta. The Brook et al. (2014) abundance matching is over plotted as a cyan solid line, and as a dashed line in the region where it has been extrapolated beyond the completeness limit of the LG.

The background color scheme indicates the regions of the $M_{star}$-$M_{halo}$ space where we expect to find cusps ($\gamma = -1.0$, in red) or progressively shallower cores (with cored-most galaxies having $\gamma = 0.0$, in black). Moving along the dark area in our map, we are moving in a region of constant $M_{star}/M_{halo} \sim 0.004$, which is where we expect to find the cored most galaxies in our model. The bottom-right side of the plot is red, corresponding to the region of space with $M_{star}/M_{halo} \lesssim 0.0001$: galaxies in this region do not have enough energy from stellar feedback to modify their profile, and they retain the initial NFW value.

Following the abundance matching line downwards from the top right corner, we are moving from a cored region, for galaxies of about $M_{star} \sim 10^8 M_\odot$, to a cuspy area, for galaxies with $M_{star} \lesssim 10^6 M_\odot$, with galaxies in the middle populating the space of inner slopes $-0.2 \lesssim \gamma \lesssim -0.8$.

In our model, Fornax and Sculptor are housed in haloes whose mass is $M_{halo} \gtrsim 10^{10} M_\odot$, and have enough stars to be within the core transformation region. In line with our findings, several authors have argued that Sculptor and Fornax have a cored dark matter distribution (Walker & Peñarrubia 2011; Amorisco & Evans 2012; Amorisco et al. 2014b, although Strigari et al. 2014 have highlighted that a cuspy profile cannot be ruled out in Sculptor).

Fornax, with its inner slope of $\gamma = -0.39$, is the cored-most Milky Way satellite in our model that follows abundance matching predictions: it is probably the easiest satellite galaxy to reconcile with an energetic outflow scenario, given its high content in stellar mass (Peñarrubia et al. 2012; Garrison-Kimmel et al. 2013). The Sculptor galaxy has a total halo mass of $M_{halo} \sim 1.5 \times 10^{10} M_\odot$ and an inner slope of $\gamma \sim -0.65$: with such values its mass within 1.8 kpc is about $M_{1.8} \sim 3.9 \times 10^8 M_\odot$, in agreement with results from Battaglia et al. (2008), who show that that observed velocity dispersion profiles are best fitted by a cored dark matter halo, and further show that an NFW profile yields a worse fit for the metal rich star population of Sculptor.

Leo I, being scattered to the right of the abundance matching line, lives within a relatively massive halo and falls in the mild-cusp region, $\gamma = -0.76$, in agreement with results from Mateo et al. (2008). The other Milky Way dSphs's that lie on the abundance matching line, Draco, Ursa Minor and Leo II, are housed in slightly

[6] Note that here, since we are mainly interested in a comparison with the cusp/core space rather than abundance matching prediction, we did not increase the halo mass for the baryon fraction, and the $M_{halo}$ values shown are exactly those listed in Table 2.

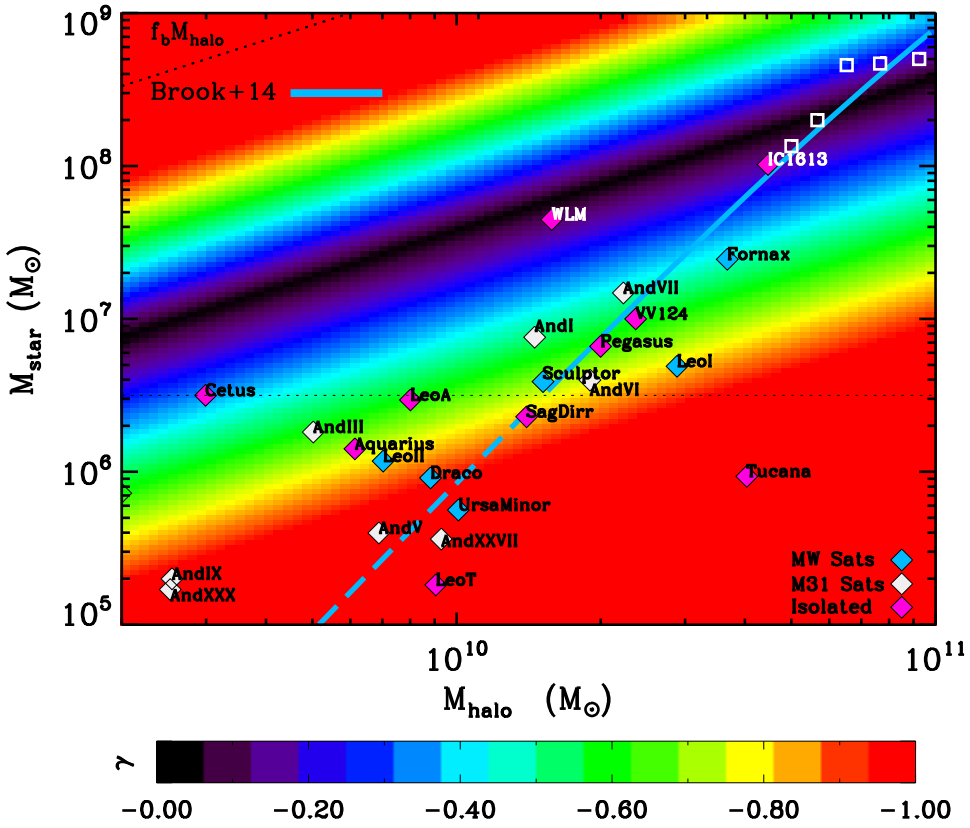


**Figure 7.** The stellar mass versus halo mass region populated by LG galaxies, assuming that they follow the mass dependent density profile DC14 proposed in Di Cintio et al. (2014b). The cyan solid line is the abundance matching prediction from Brook et al. (2014), which is well constrained down to the completeness limit of current surveys, i.e. down to a stellar mass of $10^{6.5}M_\odot$; below such limit the relation has been linearly extrapolated, and is shown as dashed cyan line. The galaxies are color coded according to their membership: Milky Way's satellites in cyan, Andromeda's satellites in white and isolated galaxies in magenta. The background image is colored according to the inner slope of dark matter profile expected for any $M_{star}/M_{halo}$ value: cuspy haloes ($\gamma = -1.0$) live in the red region, while the cored-most ones ($\gamma = 0.0$) are found in the dark area. It is immediate to see which LG member prefers cusps or cored profiles. (A color version of this figure is available in the online journal.)

smaller ($M_{halo}\sim10^{9.8-10}M_\odot$), cuspy haloes. To summarize, we find that galaxies following the abundance matching of Brook et al. (2014) (and its linear extrapolation) do not form cores in haloes below $M_{halo}\lesssim 10^{10}M_\odot$.

As discussed in Section 3.3, our model for cusp vs. core is based on the analysis of simulated isolated galaxies, and does not take into account environmental effects such as tidal disruption and ram pressure stripping. We have thus excluded the satellites circled in red in Figure 7, which may have been affected by their environment. In absence of environmental effects, the population of satellites living in the region of $M_{halo}\lesssim3\times10^9M_\odot$ would likely be shifted to higher halo masses, with the cusp/core prediction changing accordingly. Whether such disrupted galaxies should have a core or not, cannot currently be determined by our model.

A more robust analysis can be performed for the isolated galaxies in our sample, as their kinematics are not affected by any environmental process. We found that the expected cored-most galaxies should be WLM and IC1613. It has been argued that the hot stellar component of WLM may point toward a bursty star formation history that leads to a cored distribution (Teyssier et al. 2013): the agreement between the distribution of stars and gas in controlled simulations (Teyssier et al. 2013; Kawata et al. 2014) and observations (Leaman et al. 2012) supports this scenario.

VV 124, Pegasus, Leo A and Aquarius live in dark matter haloes with inner slope $\gamma\sim-0.5$. Cetus and Tucana are relative outliers, scattered either side of the abundance matching prediction. Cetus' kinematic implies that it lives in a halo with mass $M_{halo}<10^{10}M_{star}$, with inner slope $\gamma\sim-0.3$; on the contrary Tucana, with $M_{star}\sim10^6M_\odot$, has kinematics the imply a significantly more massive halo, and therefore its inferred profile is cuspy, NFW.

## 4 CONCLUSIONS

We have fit an ensemble of 40 Local Group galaxies to dark matter haloes, based on their velocity dispersions and half-light radii, which provide an estimate of their dynamical mass enclosed within $r_{1/2}$ (Kirby et al. 2014; Wolf et al. 2010). The haloes were selected from a LG halo mass function which is well described by a single power law (Brook et al. 2014). In our fiducial normalization, the LG halo mass function is set to have a maximum halo mass of $M_{halo}= 1.4\times10^{12}M_\odot$, in agreement with the most favored current mass estimates of the Milky Way and Andromeda galaxy, and resulting in a LG abundance matching that smoothly joins the large scale surveys $M_{star}$-$M_{halo}$ relation (Guo et al. 2010; Moster et al. 2013) in the region where the two volumes overlap.

Two different density profiles for dark matter haloes have been used: a cuspy NFW model (Navarro et al. 1997) and a mass dependent DC14 profile (Di Cintio et al. 2014b), which,

taking into account the impact of baryonic processes on dark matter haloes, describes the formation of shallower dark matter distributions in galaxies whose stellar-to-halo mass ratio is $0.0001 \lesssim M_{star}/M_{halo} \lesssim 0.03$ (Di Cintio et al. 2014a). The resulting best fit halo mass is shown as a function of the observed stellar mass for each galaxy in our sample, and compared with abundance matching predictions which have been empirically extended down to $M_{star} \sim 3\text{-}5 \times 10^6 M_\odot$ (Brook et al. 2014; Garrison-Kimmel et al. 2014b), in a mass range where reionization does not leave any haloes dark.

Assuming an NFW density profile, the kinematics of the sample of galaxies are best fit by relatively low mass haloes, $M_{halo} \lesssim 10^{10} M_\odot$: this results in a systematic disagreement with LG abundance matching predictions (Brook et al. 2014; Garrison-Kimmel et al. 2014b) as well as with adjusted relations that take into account the reduction of dark matter mass by up to a $30\%$ caused by baryonic effects and the fact that some low mass halo may remain dark (Sawala et al. 2015). A corollary of this mismatch is the existence of several haloes that are "too big to fail", yet have not been assigned to any observed galaxy.

A LG halo mass function with maximum halo mass of $M_{halo} = 0.8 \times 10^{12} M_\odot$ would reduce the number of "too big to fail" haloes but, although within the limits of MW and M31 mass estimates, it would require that the most massive LG galaxies are systematically matched to low halo masses, compared to the galaxies observed in larger volumes (Guo et al. 2010; Moster et al. 2013) such as in the SDSS and GAMA surveys (Baldry et al. 2008, 2012); finally, even considering such a low normalization, the disagreement between kinematically-inferred NFW halo masses and LG abundance matching predictions would remain. Whether such lower power law normalisation is the lowest possible, given the constraints of the masses of M31 and MW, is beyond the scope of this paper, and to address this point a statistical sample of Local Group simulations is required. Therefore, given the cosmic variance, our work does not rule out the possibility of having only a particularly small number of haloes with masses that are "too big to fail", although this issue was studied in detail in Garrison-Kimmel et al. (2014b).

These results confirm previous works in showing that the steep and universal NFW density profile, when combined with the halo mass function expected from collisionless cosmological simulations, do not describe well the kinematics of LG galaxies (Ferrero et al. 2012; Di Cintio et al. 2013; Tollerud et al. 2014; Garrison-Kimmel et al. 2014a; Ogiya & Burkert 2015; Collins et al. 2014).

Regardless of LG mass, the NFW model places galaxies with $10^6 \lesssim M_{star}/M_\odot \lesssim 10^8$ within haloes of $10^8 \lesssim M_{halo}/M_\odot \lesssim 5 \times 10^9$, implying a reversal of the steep trend of decreasing star formation efficiency, $M_{star}/M_{halo}$, with decreasing halo mass that is found at larger stellar masses (Guo et al. 2010; Moster et al. 2013). Considering the effects of reionization and feedback on low mass galaxies, a reversal of such trend is difficult to explain within our current theoretical framework. Indeed, models of galaxy formation, both high resolution simulations (Brook et al. 2012; Munshi et al. 2013; Shen et al. 2014; Hopkins et al. 2014) and semi-analytic models (Benson et al. 2002; Guo et al. 2011), predict that star formation efficiency will continue to decrease steeply as halo mass decreases.

To explain the high star formation efficiency of LG dwarf galaxies that arises from the NFW model, one would require a physical mechanism that allows such low mass haloes, $M_{halo} \sim 10^{8-9} M_\odot$, to have the same efficiency, in terms of $M_{star}/M_{halo}$, as haloes with mass $M_{halo} \sim 10^{11} M_\odot$. This reasoning is specially important for *isolated* LG galaxies, in which environmental effects can not be invoked to reduce their halo masses.

Yet one must consider the possibility of scatter in the $M_{star}$-$M_{halo}$ relation. Observations of luminosity functions are incomplete below a certain minimum luminosity. This means that for any given halo mass we may be seeing the high stellar mass tail of the stellar mass distribution. Thus, although the average stellar-to-halo mass relation does continue to decrease, the only galaxies that we are able to observe at the low stellar mass end may not be average. How much scatter exists in the $M_{star}$-$M_{halo}$ relation, in particular for low mass galaxies, is an open question.

Remarkably different results are found when the kinematics of the sample galaxies are described by means of the mass dependent DC14 profile.

The most massive dwarfs, those with $M_{star} \gtrsim 3\text{–}5 \times 10^6\, M_\odot$, generally fit in haloes with mass $M_{halo} \gtrsim 10^{10} M_\odot$ whose density profiles are shallower than NFW: the resulting distribution of halo masses is in agreement with abundance matching predictions and notably reduces the "too big to fail" problem in the LG.

The relation between $M_{star}$ and $M_{halo}$ for *isolated* dwarfs matches well the abundance matching relations of Brook et al. (2014); Garrison-Kimmel et al. (2014a) and their extrapolation below $M_{star} \sim 3 \times 10^6 M_\odot$, which implies that LG galaxies follow the same trend of decreasing star formation efficiency with decreasing halo mass as found for more massive galaxies in larger volumes (Guo et al. 2010; Moster et al. 2010).

Further, isolated galaxies in the DC14 model span a range of density profiles, moving from a cored region for the highest stellar mass objects, such as IC1613 and WLM, to a cuspy one for the galaxies with lowest stellar masses, such as LeoT and Tucana. The weak trend of $V_{max}$ versus $M_{star}$ pointed out in Garrison-Kimmel et al. (2014a) for the isolated galaxies in the LG is explained in the light of this result: a correlation between stellar mass and halo mass at scales smaller than $M_{star} \sim 10^8 M_\odot$ holds, but the density profiles of the haloes hosting such galaxies varies, with the brightest objects inhabiting the most massive, cored haloes, and the fainter galaxies living into smaller, cuspy haloes. Our findings therefore discard the existence of a universal profile within the haloes that host LG galaxies, in agreement with previous studies (Collins et al. 2014).

About half of the *satellite* galaxies also follow the same $M_{star}$-$M_{halo}$ relation as the isolated galaxies, with the cored most Milky Way satellites expected to be Fornax and Sculptor, in agreement with previous studies (Walker & Peñarrubia 2011; Amorisco & Evans 2012; Amorisco et al. 2014b). The other half are instead fit to lower halo masses than predicted by abundance matching, likely as a result of environmental effects (Collins et al. 2014).

The fact that no isolated galaxies prefer to live in haloes with $M_{halo} \lesssim 5 \times 10^9 M_\odot$ favors the scenario in which the environment have affected the kinematics of this subset of satellite galaxies: it seems likely that they where housed in more massive haloes prior to infall, and have had their masses reduced by the effects of ram pressure stripping, baryon outflows and/or tides (Peñarrubia et al. 2010; Zolotov et al. 2012; Arraki et al. 2014; Brooks & Zolotov 2014).

Asides from the signatures of tides that these galaxies show (Okamoto et al. 2012; Battaglia et al. 2011, 2012), another reason to favor environmental effects is that, if the mass of these objects was higher than their kinematics imply, their star formation efficiency $M_{star}/M_{halo}$ can be reconciled with the one found amongst the isolated members of the LG. Finally, acknowledging that some of the lowest mass ($M_{star} \lesssim 3 \times 10^6 M_\odot$) satellite galaxies may have been more massive in the past, helps solving the "too big to fail" problem as well, as they would populate some of the haloes

more massive than $M_{halo} \sim 7 \times 10^9 M_\odot$. Future surveys, both blind HI as well as deep optical studies, will possibly identify some yet-undiscovered faint galaxy in the nearby universe further increasing the agreement with theoretical expectations.

The existence of a cusp/core transformation amongst LG galaxies is able to explain and reconcile *at the same time* the measured shallow dark matter profile in some of the LG members, the "too big to fail" problem, the abundance matching predictions and the star formation efficiency of such galaxies.

We have shown that a combination of feedback-driven halo expansion and environmental processes within a ΛCDM context can account for the observed kinematics of Local Group galaxies, providing the theoretical framework to understand the inferred non-universality of their density profiles.

Detailed kinematical data of a larger sample, particularly of isolated galaxies, will provide crucial tests of our model.

## ACKNOWLEDGEMENTS

The authors thank the MICINN (Spain) for the financial support through the MINECO grant AYA2012-31101. They further thank Alyson Brooks and an anonymous referee for their thoughtful comments which improved the quality of the paper.

## REFERENCES

Amorisco N. C., Evans N. W., 2012, MNRAS, 419, 184
Amorisco N. C., Evans N. W., van de Ven G., 2014a, Nature, 507, 335
Amorisco N. C., Zavala J., de Boer T. J. L., 2014b, ApJ, 782, L39
Arraki K. S., Klypin A., More S., Trujillo-Gomez S., 2014, MNRAS, 438, 1466
Baldry I. K., Driver S. P., Loveday J., Taylor E. N., Kelvin L. S., et al., 2012, MNRAS, 421, 621
Baldry I. K., Glazebrook K., Driver S. P., 2008, MNRAS, 388, 945
Battaglia G., Helmi A., Tolstoy E., Irwin M., Hill V., Jablonka P., 2008, ApJ, 681, L13
Battaglia G., Irwin M., Tolstoy E., de Boer T., Mateo M., 2012, ApJ, 761, L31
Battaglia G., Tolstoy E., Helmi A., Irwin M., Parisi P., Hill V., Jablonka P., 2011, MNRAS, 411, 1013
Behroozi P. S., Wechsler R. H., Conroy C., 2013, ApJ, 770, 57
Benson A. J., Frenk C. S., Lacey C. G., Baugh C. M., Cole S., 2002, MNRAS, 333, 177
Binney J., Gerhard O., Silk J., 2001, MNRAS, 321, 471
Boylan-Kolchin M., Bullock J. S., Kaplinghat M., 2011, MNRAS, 415, L40
Boylan-Kolchin M., Bullock J. S., Kaplinghat M., 2012, MNRAS, 2657
Boylan-Kolchin M., Bullock J. S., Sohn S. T., Besla G., van der Marel R. P., 2013, ApJ, 768, 140
Breddels M. A., Helmi A., 2013, A&A, 558, A35
Brook C. B., Di Cintio A., Knebe A., Gottlöber S., Hoffman Y., Yepes G., Garrison-Kimmel S., 2014, ApJ, 784, L14
Brook C. B. et al., 2011, MNRAS, 595
Brook C. B., Stinson G., Gibson B. K., Wadsley J., Quinn T., 2012, MNRAS, 424, 1275
Brooks A. M., Zolotov A., 2014, ApJ, 786, 87
Bryan G. L., Norman M. L., 1998, ApJ, 495, 80
Bullock J. S., Kolatt T. S., Sigad Y., Somerville R. S., Kravtsov A. V., Klypin A. A., Primack J. R., Dekel A., 2001, MNRAS, 321, 559
Bullock J. S., Kravtsov A. V., Weinberg D. H., 2000, ApJ, 539, 517
Cole S., et al., 2005, MNRAS, 362, 505
Collins M. L. M. et al., 2014, ApJ, 783, 7
Corbelli E., Lorenzoni S., Walterbos R., Braun R., Thilker D., 2010, A&A, 511, A89
Côté S., Carignan C., Freeman K. C., 2000, AJ, 120, 3027
de Blok W. J. G., McGaugh S. S., Bosma A., Rubin V. C., 2001, ApJ, 552, L23
Di Cintio A., Brook C. B., Macciò A. V., Stinson G. S., Knebe A., Dutton A. A., Wadsley J., 2014a, MNRAS, 437, 415
Di Cintio A., Brook C. B., Dutton A. A., Macciò A. V., Stinson G. S., Knebe A., 2014b, MNRAS, 441, 2986
Di Cintio A., Knebe A., Libeskind N. I., Brook C., Yepes G., Gottlöber S., Hoffman Y., 2013, MNRAS, 431, 1220
Diaz J. D., Koposov S. E., Irwin M., Belokurov V., Evans N. W., 2014, MNRAS, 443, 1688
Dooley G. A., Griffen B. F., Zukin P., Ji A. P., Vogelsberger M., Hernquist L. E., Frebel A., 2014, ApJ, 786, 50
Dutton A. A., Macciò A. V., 2014, MNRAS, 441, 3359
Ferrero I., Abadi M. G., Navarro J. F., Sales L. V., Gurovich S., 2012, MNRAS, 425, 2817
Garrison-Kimmel S., Boylan-Kolchin M., Bullock J. S., Kirby E. N., 2014a, MNRAS, 444, 222
Garrison-Kimmel S., Boylan-Kolchin M., Bullock J. S., Lee K., 2014b, MNRAS, 438, 2578
Garrison-Kimmel S., Rocha M., Boylan-Kolchin M., Bullock J. S., Lally J., 2013, MNRAS, 433, 3539
González R. E., Kravtsov A. V., Gnedin N. Y., 2014, ApJ, 793, 91
Gottlöber S., Hoffman Y., Yepes G., 2010, in High Performance Computing in Science and Engineering, S. Wagner, M. Steinmetz, A. Bode, M.M. Müller, ed., Springer, pp. 309–323
Governato F. et al., 2012, MNRAS, 422, 1231
Guo Q., Cole S., Eke V., Frenk C., 2011, MNRAS, 417, 370
Guo Q., White S., Li C., Boylan-Kolchin M., 2010, MNRAS, 404, 1111
Hopkins P. F., Kereš D., Oñorbe J., Faucher-Giguère C.-A., Quataert E., Murray N., Bullock J. S., 2014, MNRAS, 445, 581
Ibata R., Chapman S., Irwin M., Lewis G., Martin N., 2006, MNRAS, 373, L70
Ibata R. A., Gilmore G., Irwin M. J., 1994, Nature, 370, 194
Jarosik N., et al., 2011, ApJS, 192, 14
Kafle P. R., Sharma S., Lewis G. F., Bland-Hawthorn J., 2012, ApJ, 761, 98
Kafle P. R., Sharma S., Lewis G. F., Bland-Hawthorn J., 2014, ApJ, 794, 59
Kahn F. D., Woltjer L., 1959, ApJ, 130, 705
Kannan R., Stinson G. S., Macciò A. V., Brook C., Weinmann S. M., Wadsley J., Couchman H. M. P., 2014, MNRAS, 437, 3529
Kawata D., Gibson B. K., Barnes D. J., Grand R. J. J., Rahimi A., 2014, MNRAS, 438, 1208
Kirby E. N., Bullock J. S., Boylan-Kolchin M., Kaplinghat M., Cohen J. G., 2014, MNRAS, 439, 1015
Klypin A., Gottlöber S., Kravtsov A. V., Khokhlov A. M., 1999, ApJ, 516, 530
Klypin A., Karachentsev I., Makarov D., Nasonova O., 2014, ArXiv e-prints, arXiv:1405.4523

Klypin A., Zhao H., Somerville R. S., 2002, ApJ, 573, 597
Koposov S. et al., 2008, ApJ, 686, 279
Kravtsov A., 2010, Advances in Astronomy, 2010
Kuhn J. R., Smith H. A., Hawley S. L., 1996, ApJ, 469, L93
Kuzio de Naray R., McGaugh S. S., de Blok W. J. G., 2008, ApJ, 676, 920
Leaman R. et al., 2012, ApJ, 750, 33
Li Y.-S., White S. D. M., 2008, MNRAS, 384, 1459
Lora V., Grebel E. K., Sánchez-Salcedo F. J., Just A., 2013, ApJ, 777, 65
Madau P., Shen S., Governato F., 2014, ApJ, 789, L17
Martin C. L., Shapley A. E., Coil A. L., Kornei K. A., Bundy K., Weiner B. J., Noeske K. G., Schiminovich D., 2012, ApJ, 760, 127
Mashchenko S., Wadsley J., Couchman H. M. P., 2008, Science, 319, 174
Mateo M., Olszewski E. W., Walker M. G., 2008, ApJ, 675, 201
McMonigal B. et al., 2014, MNRAS, 444, 3139
Merritt D., Graham A. W., Moore B., Diemand J., Terzić B., 2006, AJ, 132, 2685
Miller S. H., Ellis R. S., Newman A. B., Benson A., 2014, ApJ, 782, 115
Moore B., 1994, Nature, 370, 629
Moore B., Ghigna S., Governato F., Lake G., Quinn T., Stadel J., Tozzi P., 1999, ApJ, 524, L19
Moster B. P., Naab T., White S. D. M., 2013, MNRAS, 428, 3121
Moster B. P., Somerville R. S., Maulbetsch C., van den Bosch F. C., Macciò A. V., Naab T., Oser L., 2010, ApJ, 710, 903
Munshi F. et al., 2013, ApJ, 766, 56
Navarro J. F., Frenk C. S., White S. D. M., 1996, ApJ, 462, 563
Navarro J. F., Frenk C. S., White S. D. M., 1997, ApJ, 490, 493
Navarro J. F., Steinmetz M., 1997, ApJ, 478, 13
Obreja A., Brook C. B., Stinson G., Domínguez-Tenreiro R., Gibson B. K., Silva L., Granato G. L., 2014, MNRAS, 442, 1794
Ogiya G., Burkert A., 2015, MNRAS, 446, 2363
Ogiya G., Mori M., 2014, ApJ, 793, 46
Oh S.-H., Brook C., Governato F., Brinks E., Mayer L., de Blok W. J. G., Brooks A., Walter F., 2011a, AJ, 142, 24
Oh S.-H., de Blok W. J. G., Brinks E., Walter F., Kennicutt, Jr. R. C., 2011b, AJ, 141, 193
Okamoto S., Arimoto N., Yamada Y., Onodera M., 2012, ApJ, 744, 96
Okamoto T., Frenk C. S., 2009, MNRAS, 399, L174
Oppenheimer B. D., Davé R., 2008, MNRAS, 387, 577
Papastergis E., Giovanelli R., Haynes M. P., Shankar F., 2015, A&A, 574, A113
Peñarrubia J., Benson A. J., Walker M. G., Gilmore G., McConnachie A. W., Mayer L., 2010, MNRAS, 406, 1290
Peñarrubia J., Ma Y.-Z., Walker M. G., McConnachie A., 2014, MNRAS, 443, 2204
Peñarrubia J., McConnachie A. W., Navarro J. F., 2008, ApJ, 672, 904
Peñarrubia J., Pontzen A., Walker M. G., Koposov S. E., 2012, ApJ, 759, L42
Pontzen A., Governato F., 2012, MNRAS, 421, 3464
Purcell C. W., Zentner A. R., 2012, Journal of Cosmology and Astro-Particle Physics, 12, 7
Read J. I., Gilmore G., 2005, MNRAS, 356, 107
Salucci P., Burkert A., 2000, ApJ, 537, L9
Sawala T. et al., 2015, MNRAS, 448, 2941
Shen S., Madau P., Conroy C., Governato F., Mayer L., 2014, ApJ, 792, 99
Simon J. D., Bolatto A. D., Leroy A., Blitz L., Gates E. L., 2005, ApJ, 621, 757
Somerville R. S., 2002, ApJ, 572, L23
Stinson G. S., Brook C., Macciò A. V., Wadsley J., Quinn T. R., Couchman H. M. P., 2013, MNRAS, 428, 129
Strigari L. E., Frenk C. S., White S. D. M., 2014, ArXiv e-prints, arXiv:1406.6079
Teyssier R., Pontzen A., Dubois Y., Read J. I., 2013, MNRAS, 429, 3068
Thomas J. et al., 2011, MNRAS, 415, 545
Tollerud E. J., Boylan-Kolchin M., Bullock J. S., 2014, MNRAS, 440, 3511
Tollerud E. J., Bullock J. S., Strigari L. E., Willman B., 2008, ApJ, 688, 277
van der Marel R. P., Fardal M., Besla G., Beaton R. L., Sohn S. T., Anderson J., Brown T., Guhathakurta P., 2012, ApJ, 753, 8
Walker M. G., Mateo M., Olszewski E. W., Peñarrubia J., Wyn Evans N., Gilmore G., 2009, ApJ, 704, 1274
Walker M. G., Peñarrubia J., 2011, ApJ, 742, 20
Watkins L. L., Evans N. W., An J. H., 2010, MNRAS, 406, 264
Weiner B. J. et al., 2009, ApJ, 692, 187
Weisz D. R., Dolphin A. E., Skillman E. D., Holtzman J., Gilbert K. M., Dalcanton J. J., Williams B. F., 2014, ApJ, 789, 147
Wolf J., Martinez G. D., Bullock J. S., Kaplinghat M., Geha M., Muñoz R. R., Simon J. D., Avedo F. F., 2010, MNRAS, 406, 1220
Woo J., Courteau S., Dekel A., 2008, MNRAS, 390, 1453
Zolotov A. et al., 2012, ApJ, 761, 71

This paper has been typeset from a TEX/ LATEX file prepared by the author.